2006 ASME Joint U.S. - European Fluids Engineering Summer Meeting
July 17-20, Miami, FL

FEDSM2006-98467

LATTICE BOLTZMANN THERMAL FLOW SIMULATION AND MEASUREMENTS OF A MODIFIED SAE MODEL WITH HEATED PLUG

Ehab Fares*
Exa GmbH, Curiestrasse 4,
D-70563 Stuttgart, Germany
Email: ehab@exa.com

Sacha Jelic
Exa GmbH, Curiestrasse 4,
D-70563 Stuttgart, Germany
Email: sacha@exa.com

Timo Kuthada
FKFS Research Institute
Pfaffenwaldring 12, D-70569 Stuttgart, Germany

David Schröck
FKFS Research Institute
Pfaffenwaldring 12, D-70569 Stuttgart, Germany

ABSTRACT

This article presents the novel experiment of the modified SAE model with a heated plug and discusses the details about the new developments of the numerical model of the PowerFLOW 4.0 version, which employs a Lattice Boltzmann model and incorporates an improved unsteady two equations RNG k-ε turbulence model, a coupled PDE for the energy equation and an advanced wall model for both flow and thermal boundary layers.
The hot flow is discussed both experimentally and numerically. Distributions of the flow field are compared with available experimental findings. The predictive capability and the feasibility of the current Lattice Boltzmann approach is demonstrated and the applicability to similar flows over realistic road vehicles is discussed.

INTRODUCTION

Increasingly stricter automotive thermal management requirements, tighter packaging and rising component temperatures in the underhood and underbody of a vehicle are thermally demanding in the development of a new vehicle. Thermal shielding or even design modifications at a late stage of the development cycle represent considerable costs and delays. An accurate and feasible prediction of the flow field including all heat transfer modes such as forced/natural convection, conduction and radiation using numerical methods constitute an early and a much cheaper alternative to windtunnel or road testing. However, such a complex simulation constitutes a considerable challenge to available numerical methods [1]. As part of a comprehensive validation effort of the Lattice Boltzmann based software PowerFLOW 4.0 for automotive thermal management applications an experimental and numerical study of the modified SAE-type K body is conducted. The SAE body [2] is modified to accommodate an engine compartment with a simplified engine block and a radiator [3]. Furthermore, a heated pipe within the cooling air evacuation duct in the underbody representing a simplified model of the exhaust system of a vehicle is also included. Measurements of surface pressure and temperatures as well as field measurements of velocities and temperatures in the relevant areas especially near the heated pipe are used to validate the new numerical approach for hot flows. Recent validations of the current numerical approach for both academic [1] and complex underhood cold flows are documented e.g. in [4] and demonstrate the capability of the underlying method to capture the correct flow behavior even for the complex and geometrically detailed case.

*Address all correspondence to this author.

NUMERICAL METHOD

The numerical simulations are carried out using the PowerFLOW 4.0 software based on the Lattice Boltzmann model. Previous versions based on the thermal lattice gas automata were validated in many publications for a wide variety of applications [5–10]. Results using the new version are documented e.g. in [1, 11].

Thermal Lattice Boltzmann Approach

The D3Q19 Lattice Boltzmann model [12–17] with the BGK collision approximation [18] is defined as

$$f_i(\mathbf{x}+\xi_i\Delta t, t+\Delta t) = f_i(\mathbf{x},t) + \frac{\Delta t}{\tau}\cdot(F_i(\mathbf{x},t) - f_i(\mathbf{x},t)) \quad (1)$$

with the equilibrium distributions F_i (approximated up to third order [19–21]) defined according to

$$F_i = \rho_l w_i \left[1 + \frac{\xi_i\cdot\mathbf{u}_l}{T_l} + \frac{(\xi_i\cdot\mathbf{u}_l)^2}{2T_l^2} - \frac{\mathbf{u}_l^2}{2T_l} + \frac{(\xi_i\cdot\mathbf{u}_l)^3}{6T_l^3} - \frac{\xi_i\cdot\mathbf{u}_l^3}{2T_l^2}\right] \quad (2)$$

using the weighting factors w_i equal to $1/3$, $1/36$ and $1/18$ for the rest particles, the 12 bi-diagonal directions and the 6 coordinate directions, respectively and the particles velocities ξ_i of the distributions f_i in direction i. The particles velocities ξ_i are chosen in such a way, that the $\xi_i\Delta t$ corresponds to a simultaneous propagation of the particle distributions f_i to the neighboring lattice sites in direction i. The relaxation time τ is determined according to the molecular viscosity

$$\tau = \nu_l/T_l + \Delta t/2 \quad . \quad (3)$$

Macroscopic hydrodynamic quantities such as density ρ_l or momentum density $\rho_l\mathbf{u}_l$, all in lattice units denoted by the subscript $(\,)_l$, can be obtained using moments of the distribution functions

$$\rho_l(\mathbf{x},t) = \sum_i f_i(\mathbf{x},t) \quad and \quad \rho_l\mathbf{u}_l(\mathbf{x},t) = \sum_i \xi_i f_i(\mathbf{x},t) \quad . \quad (4)$$

Similarly the momentum tensor is calculated using

$$p_l\delta_{jk} + \rho_l u_{lj} u_{lk} = \sum_i \xi_{i,j}\xi_{i,k} F_i(\mathbf{x},t) \quad . \quad (5)$$

All the variables in lattice units can be mapped to physical units, e.g. in mks units, according to simple scaling rules. The choice of the lattice temperature $T_l = T_l = 1/3$ is mainly for stability reasons [22] and leads after evaluation of (5) [23] to the relation

$$p_l = R_l\rho_l T_l \quad \text{with} \quad R_l = 1 \quad (\gamma_l = 1) \quad (6)$$

for the pressure p_l and a constant lattice sound speed $a_l = \sqrt{\gamma_l R_l T_l} = 1/\sqrt{3}$.

Using the Chapman-Enskog expansion [24] the compressible Navier-Stokes equations can be derived. However, in contrast to the Navier-Stokes equations the *LBGK* defined through equation (1) is linear and relies on simple computational operations for advection and collision allowing for both an efficient and accurate implementation, which is one of the main advantages over other computational fluid dynamics (CFD) solvers based on finite difference or finite volume discretizations. Furthermore, the local computational nature of the *LBGK* makes its solution algorithm an excellent candidate for parallelization.

It is possible in general to extend the Lattice Boltzmann model to simulate non-isothermal flows satisfying the ideal gas equation and energy balance. The extension necessitates the introduction of a set of new degrees of freedom to the lattice states leading to variations such as the D3Q34 (former PowerFLOW model) and D3Q54 [25]. Besides the obvious added computational effort as a consequence of added Lattice speeds these approaches have more stability restrictions [22] and hence practically limit the temperature ranges $T_{max} \approx 2\cdot T_{char}$ [26]. Another more general and viable approach using a scalar transport equation for the temperature coupled with the Lattice Boltzmann solver is hence applied here. The partial differential equation for conservation of energy can be reformulated in terms of temperature [27]

$$\rho c_p\left(\frac{\partial T}{\partial t} + \vec{u}\cdot\nabla T\right) = \nabla\cdot(\lambda\nabla T) + \dot{Q} + \beta T\frac{Dp}{Dt} + \Phi \quad . \quad (7)$$

It can be shown that both the pressure derivative and the dissipation term, i.e. the last two terms, can be neglected [28] for slightly compressible flows at moderate speeds $Ma \ll 1$.

The heat conductivity λ can be also defined via the constant Prandtl number $Pr = \mu c_p/\lambda$. It is known experimentally [29] that $Pr \approx 0.71$ for air is constant over a wide range of temperatures, i.e. the heat conductivity scale similarly with temperature as the molecular dynamic viscosity. This definition enables furthermore the extension to turbulent flow via the Boussinesq hypothesis [30] for an *effective* viscosity μ_{eff} and hence an effective heat conductivity λ_{eff} as a sum of a molecular and a turbulent component determined through a turbulence model and used to define an effective relaxation time of equation (3)

$$\mu_{eff} = \mu + \mu_t \quad \Rightarrow \quad \lambda_{eff} = \lambda + \lambda_t = \frac{\mu c_p}{Pr} + \frac{\mu_t c_p}{Pr_t} \quad . \quad (8)$$

This introduces also the new dimensionless turbulent Prandtl number Pr_t. Very often this value is also assumed to be constant [30], i.e. $Pr_t = 0.9$ for air. However, it is known that this assumption is not valid through the thermal boundary layer and differences exist between e.g. the the free mixing jet and the wall boundary layers [30]. The heat transfer predictions can be improved using a dynamically determined Pr_t similar to [31]. The PDE for the temperature evolution can be summarized as

$$\rho c_p\frac{DT}{Dt} = \nabla\cdot\left((\frac{\mu c_p}{Pr} + \frac{\mu_t c_p}{Pr_t})\nabla T\right) + \dot{Q} \quad . \quad (9)$$

This equation is solved using a Lax-Wendroff second-order finite difference scheme similar to the discretization of the used $k-\varepsilon$ RNG turbulence model [32] described later.

The abovementioned PDE takes into account the temperature variation of the fluid due to various heat sources such as a

heat exchangers of heat transfer from a hot surface. If the temperature change is not coupled to the momentum equation, i.e.the *LBE*, then it will act as a "passive scalar" and is expected to reproduce the correct flow behavior for moderate temperature ranges $\Delta T \sim 100°C$, where expected density variations remain small. According to the Boussinesq approximation [28] for moderate temperature ranges all flow properties are assumed to be temperature independent with an addition for a virtual volumetric force describing the buoyancy due to the temperature driven density variation [26]. The "active" feedback into the momentum equation results in change of density and hence extends the range of temperatures that can be simulated considerably. Furthermore, this implementation naturally takes into account buoyancy effects in the flow. There are several ways to achieve this, either by directly manipulating the equilibrium distributions F_i in order to retain the ideal gas equation (6) for the varying temperature T, or in the manner similar to the work in [33].

Turbulence Modeling

In the underlying approach a k-ε turbulence model is incorporated into the *LBE* [34]. The original two equation Renormalization Group (RNG) k-ε [35] is modified [32, 36]

$$\rho\frac{Dk}{Dt} = \frac{1}{\sigma}\frac{\partial}{\partial x_j}\left[(\mu+\mu_t)\frac{\partial k}{\partial x_j}\right] + \tau_{ij}S_{ij} - \rho\varepsilon \tag{10}$$

$$\rho\frac{D\varepsilon}{Dt} = \frac{1}{\sigma}\frac{\partial}{\partial x_j}\left[(\mu+\mu_t)\frac{\partial \varepsilon}{\partial x_j}\right] + C_{\varepsilon_1}\frac{\varepsilon}{k}\tau_{ij}S_{ij} - \left[C_{\varepsilon_2} + C_\mu\frac{\eta^3(1-\eta/\eta_0)}{1+\beta\eta^3}\right]\rho\frac{\varepsilon^2}{k} \tag{11}$$

with k representing the turbulence kinetic energy, ε the turbulent dissipation, τ_{ij} the stress tensor, S_{ij} the strain rate tensor defined as

$$\tau_{ij} = 2\mu_t S_{ij} - \frac{2}{3}\rho k\delta_i j \quad S_{ij} = \frac{1}{2}\left(\frac{\partial u_i}{\partial x_j} + \frac{\partial u_j}{\partial x_i}\right) \quad \mu_t = \rho C_\mu\frac{k^2}{\varepsilon} \tag{12}$$

the closure coefficients

$$C_\mu = 0.085 \quad C_{\varepsilon_1} = 1.42 \quad C_{\varepsilon_2} = 1.68$$
$$\sigma = 0.719 \quad \eta_0 = 4.38 \quad \beta = 0.012 \tag{13}$$

and the closure function η modified to be a function of the dimensionless shear rate $|S|k/\varepsilon$ and the dimensionless vorticity $|\Omega|k/\varepsilon$ using $\Omega_{ij} = 1/2(\partial u_i/\partial x_j - \partial u_j/\partial x_i)$ [32, 36]. This swirl correction together with the inherently unsteady nature of the lattice Boltzmann equation adequately reproduces the large vortices. This represents, from a pragmatic point of view [37] the key factor in predicting *LES* similar solutions on coarse grids using an unsteady turbulence model, a methodology referred to as very large eddy simulation (VLES). Note also that the *LBGK* approach possesses from a conceptual point of view an advantageous representation of fluid turbulence over the solution of the Navier-Stokes equations due to it's computationally efficient formulation [38].

The turbulence model is solved on the same grid used for the lattice Boltzmann simulation using an explicit Lax-Wendroff second-order finite difference scheme [32]. The equations are linked to the lattice Boltzmann simulation through the turbulent viscosity $\nu_t = \mu_t/\rho$ which now is added to the molecular viscosity ν in equation (3) according to the Boussinesq hypothesis.

Boundary Conditions and Wall model

Inflow/Outflow Inflow or outflow boundary conditions based on simple extrapolations or simplified characteristics is easily defined using the assumption of local equilibrium $f_i \equiv F_i$ on the boundary. Usually velocity and turbulence kinetic energy is imposed at the inflow boundaries, whereas the static pressure is kept constant at the outflow. Other values are extrapolated from the simulation domain. The boundary conditions is implemented in an under relaxation manner to avoid large local gradients especially during the startup process. Therefore, the prescribed values are not fixed but may change slightly according to the local flow behavior.

Wall Treatment

Lattice Boltzmann Wall BC The standard bounce back boundary condition for no slip or the specular reflection for free slip condition does not produce accurate results on non-lattice aligned curved surfaces. Higher order interpolation modifications have been proposed [39] but still do not give satisfactory smooth results. The boundary condition applied here is based on a volumetric formulation near the wall [40]. The surface is facetized within each volume element *Voxel* intersecting the wall geometry using planar surface elements *Surfels*. A particle bounce back or specular reflection is performed on each of them and further linear interpolation and weighted averaging ensures the conservation of mass and momentum [11, 40], which is shown to achieve vanishingly small numerical friction along an arbitrarily oriented flat surface and across *VR*s. This is essential for realizing the wall turbulent momentum flux requirements.

Wall Model Boundary layers at high Re numbers possess much higher gradients in the normal directions than the streamwise direction. However, in many cases the details within the wall bounded boundary layer are not relevant and algebraic relations such as the logarithmic law of the wall can be used to derive a wall model [27, 32, 36] to implicitly calculate the friction velocity u_τ and turbulent quantities at the first cell center near the wall at a normalized wall distance $y^+ > 30$. This is based on the universality of the near wall behavior of the turbulent boundary layer as documented in many works. e.g. [27, 41]. The current formulation is an extension to the standard wall model

formulation

$$u_\tau = \sqrt{\frac{\tau_{wall}}{\rho}} \qquad y^+ = \frac{y u_\tau}{\nu}$$

$$\frac{u_t}{u_\tau} = f(y u_\tau/\nu, k_s, \xi(\nabla p) \qquad k = \frac{u_\tau^2}{\sqrt{C_\mu}} \qquad \varepsilon = \frac{u_\tau^4}{\nu \kappa y^+} \quad (14)$$

where u_τ represents the skin friction velocity and y^+ the dimensionless normal distance of the wall evaluated at the center of the first cell and using the local tangential component of velocity u_t, the normal wall distance y and a surface roughness length k_s. The function $\xi(\nabla p)$ includes the influence of adverse and favorable pressure gradients. The wall model has been validated for a number of applications such as [9, 42] and was formulated to additionally account for the sensitive pressure induced separations.

The thermal boundary layer is handled similarly using

$$T^+ = \frac{(T_{wall} - T_{near\_wall}) \rho c_p u_\tau}{q_{wall}} \quad (15)$$

based on the wall temperature T_{wall} the wall heatflux q_{wall} and the near wall temperatures T_{near_wall} evaluated at the center of the first voxel away from the wall according to the temperature PDE (9). The thermal wall model is defined as [26, 27]

$$T^+ = A \ln y^+ + F(Pr) \quad (16)$$

where A represents a constant and $F(Pr)$ a function of the local Pr number. A further modification to account for the viscous regime $y^+ < 30$ is also included similar to the fluid viscous sublayer $u^+ = y^+$. Equations (15,16) relate the near wall temperatures T_{near_wall} with the wall temperatures T_{wall} and the wall heat fluxes q_{wall}. Therefore, the wall model can be used either to determine the wall heat flux if the wall temperatures are given as a surface boundary condition or vice versa. A local heat transfer coefficient near the wall is easily determined

$$h_{local} = \frac{q_{wall}}{T_{wall} - T_{near\_wall}} \quad . \quad (17)$$

Grid Refinement Strategy

Local variable refinement regions *VR*s can be defined to locally allow for refinement or coarsening the grid per region by a factor of 2. The cells at every VR level are uniform in size in all directions. The transfer of the velocity distributions f_i across the *VR*s is done similar to [39, 43] but ensuring mass and momentum conservation via a volumetric formulation [44, 45].

The aforementioned discretization of the temperature and k-ε PDEs uses a non-uniform mesh formulation [32] that takes into account the *VR* transition spatially and temporally.

Porous Media Model

A porous medium representing a heat exchanger such as a radiator is characterized through a pressure drop representing the resistance to the flow

$$\frac{\partial p}{\partial x_i} = -\rho \left(V_i + I_i |\mathbf{u}|\right) u_i \quad (18)$$

where V_i and I_i represent the viscous and the inertial resistance coefficients based on the local velocity u in the i^{th} direction. This is an extension to originally linear Darcy's law [46] and is implemented through a forcing term in the *LBE* equation. In addition an added heat source can also be modeled via a constant volumetric heat or velocity dependent heat exchange coefficient.

EXPERIMENTAL SETUP

The following sections give a short overview of the used model, wind tunnel and measurement techniques.

Wind tunnel

All experimental investigations were conducted in the $IVK1:4/1:5$ model scale wind tunnel. It is a closed air circuit wind tunnel with an open jet test section. The exit nozzle cross-sectional area is $A = 1.65m^2$ with a maximum free stream velocity of $280km/h$. An additional floor was inserted for the thermal protection of the state-of-the-art 5-belt road simulation system [47].

SAE-type K model

Figure 1. SAE-type K model mounted on struts in the windtunnel

The SAE Reference Body was defined by the SAE Open Jet Interference Committee to investigate the influence of different wind tunnel parameters and to generate a simplified model for wind tunnel comparisons. This first model is made of a simplified car-shaped body held on struts, with interchangeable rear modules [48]. The SAE Model Type K [3] was later introduced at FKFS to conduct basic experiments on cooling air drag under different road simulation techniques. The model is scaled 1 : 4 and allows a variable cooling airflow through a simply shaped engine compartment as shown in figures 1 and 2. The cooling air flow path is designed to be as flexible as possible by allowing interchangeable cooling modules to be installed. The front module used for this investigation has one cooling inlet and its ratio

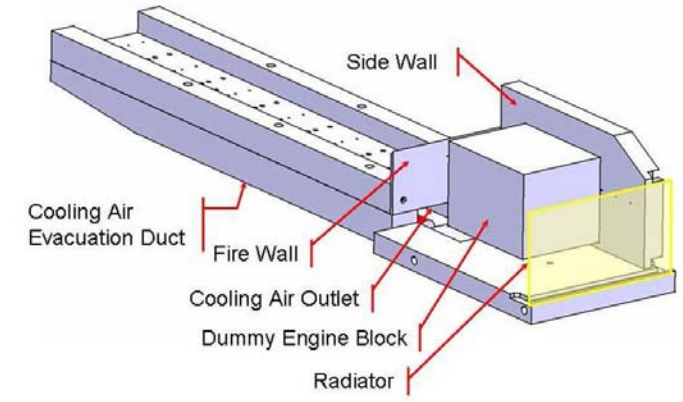

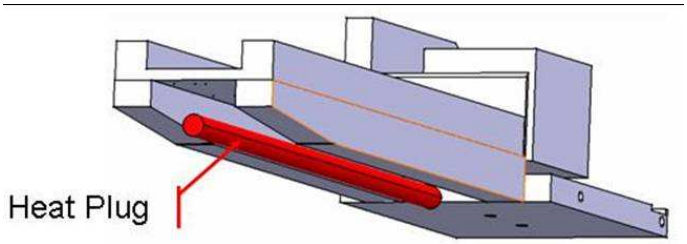

Figure 2. Internal model assembly

Figure 3. Heated plug in the underbody evacuation duct

cooling inlet area to cross sectional area is similar to that of a typical middle class car. The engine compartment was equipped with a radiator core equipped with FKFS Radiator Probes (see figure 12) for the determination of the cooling air flow rate and a simplified engine block. The accuracy for the measured cooling air volume flow is in this case approximately two per cent [49]. For the presented investigations the center tunnel, which will be referred in future as cooling air evacuation duct, was equipped with a $3kW$ heat plug to simulate the hot exhaust system as shown in figures 2 and 3.

Measurement Technique

In order to investigate the effects of the additional energy brought into the flow by the heat plug the model was equipped with a set of measuring technique. Inside the engine compartment surface pressure probes were evenly distributed along a line on the side wall at mid height. On the top surface of the cooling

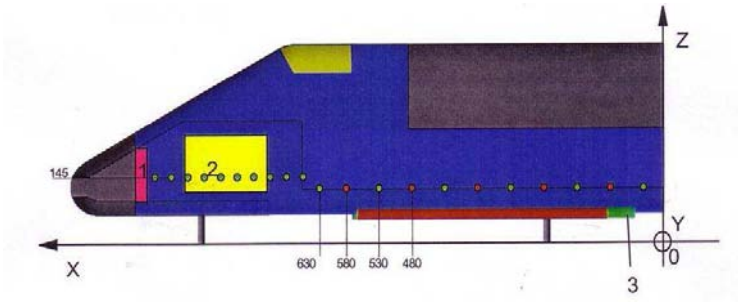

1 Radiator 2 Engine Block 3 Heat Plug

Figure 4. Measurement location of static pressure (green) and surface temperature (red)

air evacuation duct surface pressure probes and type K thermocouples to measure surface temperatures were placed alternately along three lines,i.e. at $Y = 0mm$ (centerline of the model), at $Y = 10mm$ and at $Y = 30mm$ as depicted in figure 4. Flow field temperature measurements were conducted with a sheath thermocouple that was additionally shielded from radiation with a ceramic tube that only left the tip of the thermocouple uncovered. The flow field itself was investigated with a fast response pressure probe to gain understanding of flow velocities and angles. Within the $\pm 45^\circ$ acceptance cone the accuracy of the probe is $\pm 0.6 m/s$ and $\pm 1^\circ$ for pitch and yaw angle. The pressure probe as well as the sheath thermocouple were held and moved by a traverse unit. Two measuring planes in XZ- and YZ-direction

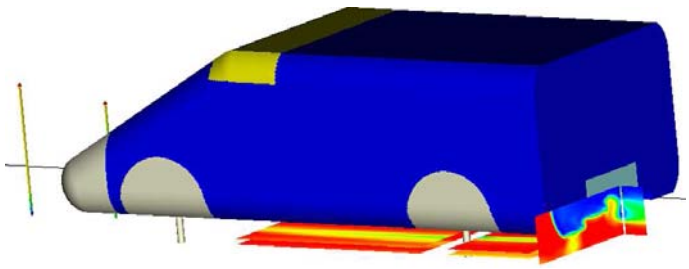

Figure 5. Inflow profiles and measurement planes in the underbody and wake region

were placed behind the model in the near wake, two planes were traversed in XY-direction at two different heights underneath the model as shown in figure 5. The grid of all measuring planes was 10-by-10 mm. Surface temperature and surface pressure measurements were made for $30s$ and then time averaged. Flow field temperatures were made for $5s$ at each measuring location. Due to the fast response characteristics of the pressure probe the so called "Flying Probe" technique could be used to determine the velocity components of the flow field [50]. In addition velocity profiles were also measured upstream of the model as indicated in figure 5 to confirm the correct inflow flow behavior later during comparison with simulations.

RESULTS AND DISCUSSION
Numerical Setup and Grid

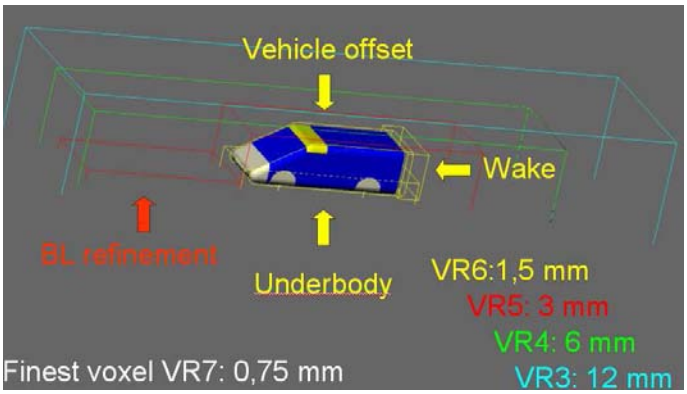

Figure 6. Simulation domain and VR setup

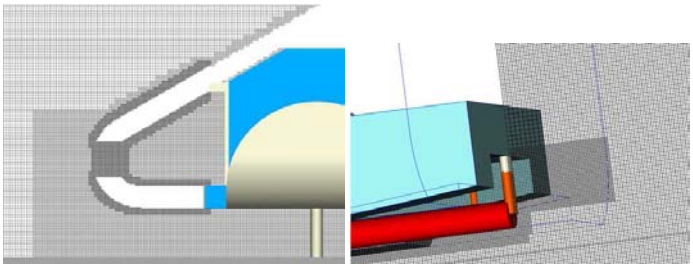

Figure 7. Computational lattice at the centerline showing the finest VR

Seven *VR* levels are used for the simulation as given in figure 6, where the finest resolution of $0.75mm$ regions are located at the model nose, evacuation duct and as an offset from the plug as depicted in figure 7. The determination of the necessary resolution followed the same length scales estimation as in [1]. Additionally a subsequent evaluation of the $y^+ < 150$ values on the surface was conducted to verify that the chosen resolution is indeed sufficient for the wall model to predict the boundary layer correctly as depicted in figure 8. The resulting grid consists of 52 million voxels and 2.4 million surfels. The automatic grid generation takes about 1.5 hours on a 2.4 GHz quad Opteron node. The simulation was run on 64 2.8 GHz Xeon processor cluster requiring a total of $20GB$ distributed memory and performing ~ 50.000 timesteps corresponding to a $\sim 0.06s$ in physical simulated time a day. The simulation was run until relevant flow parameters such as forces, the surface pressure coefficients in the engine compartment and cooling air evacuation duct and the velocity in the wake are settled which in the case presented here were settled after approximately ~ 80.000 timesteps.

Comparisons with Experiment

The case presented here has a heat plug internal thermocouple temperature $550°C$ and a free stream velocity $\sim 10m/s$. This

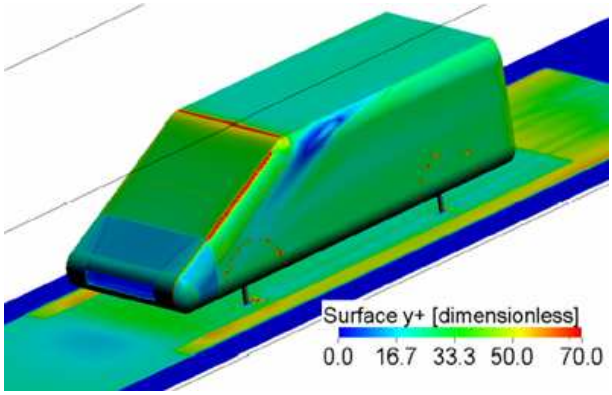

Figure 8. y^+ values on the surface

represents the most demanding case from the experimental test suite, since it has the highest temperature gradients near the plug and the lowest flow speed measured. The measured velocity field and surface pressure showed only a slight difference between the cold and hot flows, i.e. with the plug heated or left non-heated. The exhaust pipe and cooling air evacuation duct temperature distributions from experiment are shown in figures 9 and 10 respectively, which were used as a spatially varying boundary condition on the corresponding surfaces. The temperatures on the plug are only interpolated in xdirection and a constant distribution in circumferential direction on the plug is assumed. From three circumferentially distributed thermocouples at $x = 0.592m$ it is known from experiment, that a variation of $23°C$ can occur. However, relative to the average plug temperatures, this represents only 4%. To ensure the correct inflow flow behavior

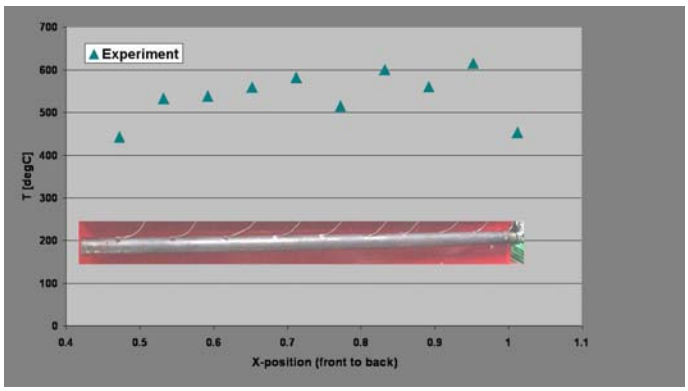

Figure 9. Measurement of surface temperatures on the heated plug

especially due to floor boundary layer a measurement of the centerline velocity profile at $20mm$ and $200mm$ in front of the model was performed. Since the simulation model did not include the complete open channel windtunnel a fictitious floor was used in the simulation with a length chosen to match the inflow velocities as indicated in figure 11. It should be noted that the probe used for the measurements is not well suited to validate the near wall

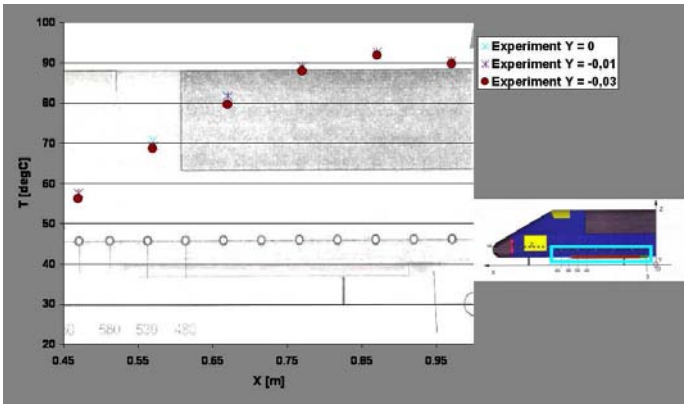

Figure 10. Measured surface temperatures in the evacuation duct at different y-positions

model boundary layer due to its diameter size. It was used only to have a general view of the incoming flow. Deviations between experiment and simulation are therefore within acceptable range.

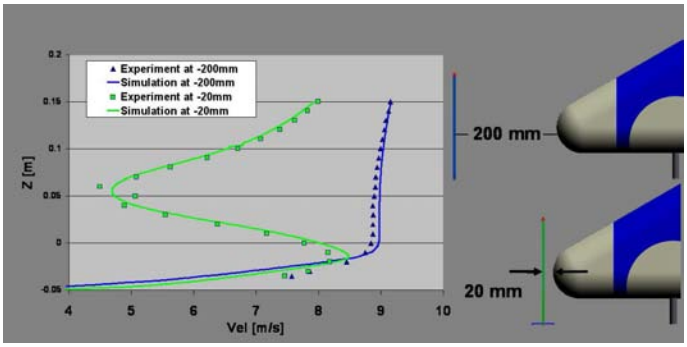

Figure 11. Comparisons of centerline inflow profiles

The velocities through the radiator are compared in figure 13. In general the simulated velocities are lower than the measurement which can be led back to geometrical sealing differences between experiment and simulation model in the region of the radiator.

The c_p values at the surface of the engine compartment sidewall and firewall are shown in figure 14. The experiment measurement accuracy is also indicated with error bars. Note that the simulation c_p- values are slightly lower than the experimental values however still marginally within the measurement accuracy domain. The c_p values in the cooling air evacuation duct shown in figure 15 are very close to experiment, except for the first point ($x = 0.42m$), which is in the separated flow area right behind the engine compartment cooling air outlet.

The velocity field measurements in the xz-wake, yz-wake and underbody at ground heights $z = 25mm$ and $35mm$ are shown in figures 16 till 19.The percentage of good data is also shown

Figure 12. Radiator core equipped with 6 Probes

Experiment			Simulation		
1.28	1.18	1.17	1.03	1.10	1.06
1.45	1.46	1.56	1.23	1.19	1.20

Figure 13. Comparisons of radiator velocities im m/s

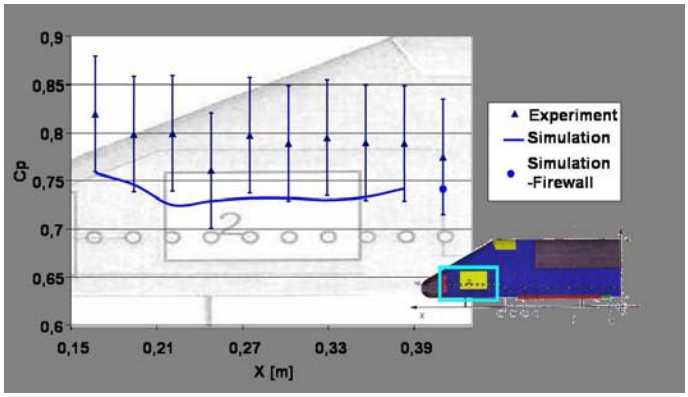

Figure 14. Comparison of pressure coefficient in the engine compartment

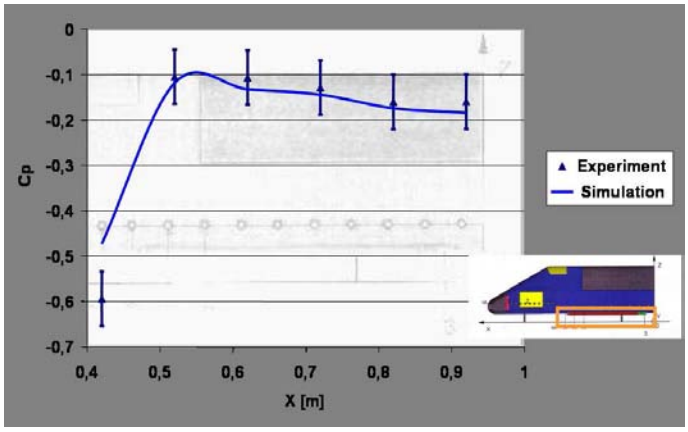

Figure 15. Comparison of pressure coefficient in the engine compartment

for the windtunnel measurements. At one position, it indicates the amount of measurements that were within a predetermined angle with respect to the probe. If the local flow velocity vector is outside this angle, it was determined as not a good data point. The results match very well for the regions where the experiment shows a high percentage of good measured data indicating the regions of backflows not measured by the probe.

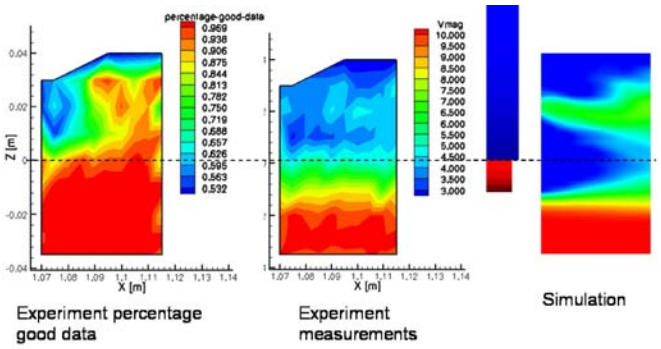

Figure 16. Comparison of the wake velocity distribution in the xz-plane

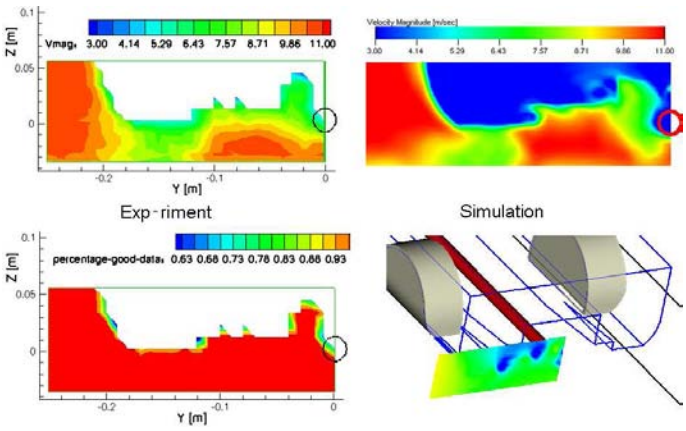

Figure 17. Comparison of the wake velocity distribution in the yz-plane

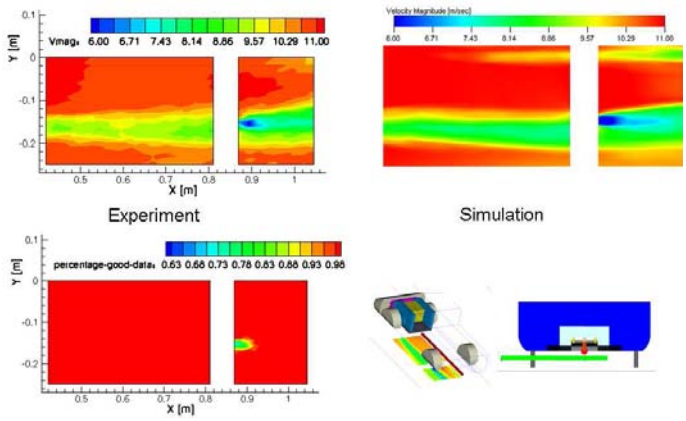

Figure 18. Comparison of the underbody velocity distribution in the xy-plane(height $25mm$)

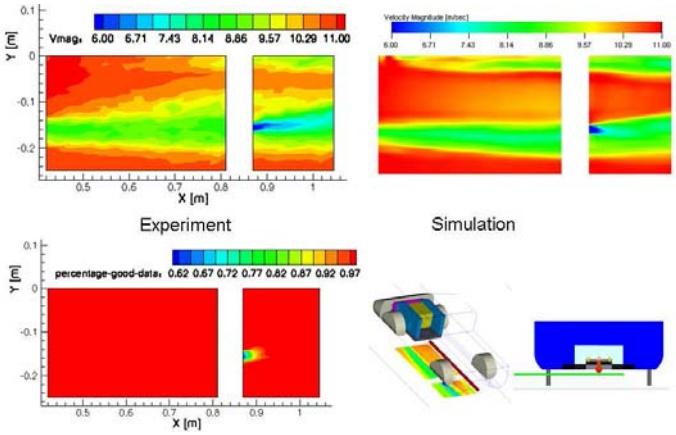

Figure 19. Comparison of the underbody velocity distribution in the xy-plane(height $35mm$)

Similarly the comparisons of the temperature field is shown in figures 20 till 22 indicating quantitatively the same temperature range and maximum temperature, however the extent of the hot plume generated by the heated plug in the vertical direction is offsetted. Since this region contains very low velocities especially in the immediate wake of the plug itself it is expected that diffusion heat transfer mechanisms may dominate locally and hence require additional physical time to develop further. This also explains why the temperatures right below the exhaust pipe are lower than experiment, since the high temperatures are not expanded to the measurement plane height.

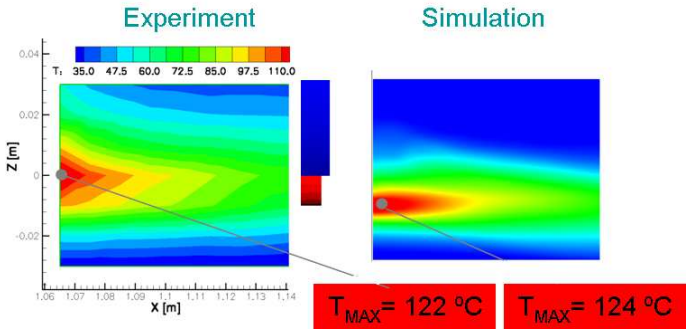

Figure 20. Comparison of the wake temperature distribution in the xz-plane

CONCLUSIONS AND OUTLOOK

The overall flow structures are accurately captured by the PowerFLOW simulation both qualitatively and quantitatively. The current numerical approach shows good results inside the cooling air evacuation duct for the surface c_p values on the upper wall. Also the results for the velocity field in the xz-wake,

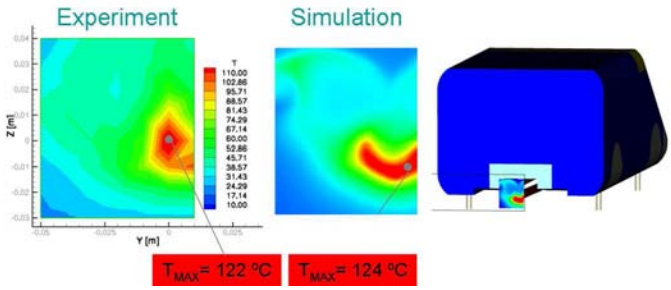

Figure 21. Comparison of the wake temperature distribution in the yz-plane

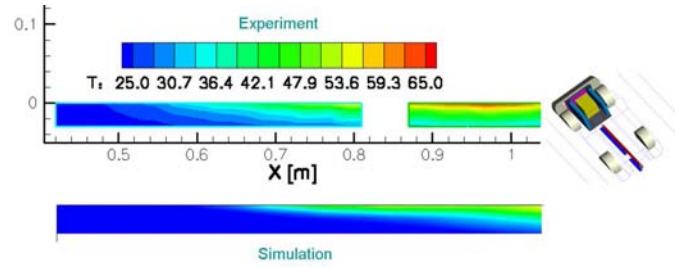

Figure 22. Comparison of the underbody temperature distribution in the xy-plane(height $25mm$)

yz-wake and xy-underbody planes are simulated accurately. The temperature field for the two planes in the wake is calculated quantitatively very accurately. However, the expansion of the temperature wake flow field in vertical direction is smaller in simulation, which is expected to improve further by longer simulation time.

This case was chosen to represent the most difficult flow of a realistic car application, i.e. high temperatures and low convective velocities. The comparisons shown here demonstrate the ability of the underlying numerical method to accurately predict the flow structures and the applicability to geometrically more complex cases is expected. Furthermore, a coupled flow simulation with a radiation/conduction tool is also being developed in order to predict both the flow and surface temperature distributions simultaneously.

REFERENCES

[1] Fares, E., 2006. "Unsteady flow simulation of the ahmed reference body using a lattice boltzmann approach". *Comput. Fluids,* **in press**.

[2] Good, G. M. L., and Garry, K. P., 2004. "On the use of reference models in automotive aerodynamics". SAE Paper 2004-01-1308.

[3] Kuthada, T., Pfannkuchen, E., and Wiedemann, J., 2004. "Evaluation of cooling air drag on a reference body". Proceedings of the 5th MIRA Int. Conference on Vehicle Aerodynamics, Warwick (UK).

[4] Baily, O., Baby, X., Fares, E., and de Portzamparc, H., 2005. "Piv and numerical correlations on the laguna 2 underhood flow field". Proceedings of the SIA Conference *Fluid Dynamics*, Lyon, 26-27 oct., Accepted for publications in Ingnieurs de l' Automobile.

[5] Anagnost, A., Alajbegovic, A., Chen, H., Hill, D., Teixeira, C., and Molving, K., 1997. "Digital Physics analysis of the Morel body in ground proximity". SAE Paper 970139.

[6] Duncan, B. D., Sengupta, R., Mallick, S., and Sims-Williams, D. B., 2002. "Numerical simulation and spectral analysis of pressure fluctuations in vehicle aerodynamic noise generation". SAE Paper 2002-01-0597.

[7] Halliday, J., and Teixeira, C., 1998. "Validating lattice-based CFD for automotive HVAC ducting systems". In Proc. of ISATA conference, Düsseldorf.

[8] Halliday, J., Teixeira, C., and Alexander, C., 1999. "Simulation of engine internal flows using Digital Physics". *Oil & Gas Science and Technology-Rev.IFP,* **54**(2), pp. 187–191.

[9] Shock, R. A., Mallick, S., Chen, H., Yakhot, V., and Zhang, R., 2002. "Recent results on two-dimensional airfoils using a lattice Boltzmann-based algorithm". *Journal of Aircraft,* **39**(3), pp. 434–439.

[10] O.Vaillant, and Maillard, V., 2003. "Numerical simulation of wall pressure fluctuation on a simplified vehicle shape". AIAA Paper 2003-3271.

[11] Li, Y., Shock, R., Zhang, R., and Chen, H., 2004. "Numerical study of flow past an impulsively started cylinder by lattice Boltzmann method". *J. Fluid Mechanics,* **519**, pp. 273–300.

[12] Abe, T., 1997. "Derivation of the lattice Boltzmann method by means of the discrete ordinate method for the Boltzmann equation". *J. Computat. Phys.,* **131**, pp. 241–246.

[13] Chen, S., Chen, H., Martinez, D., and Matthaeus, W., 1991. "Lattice Boltzmann model for simulation of magnetohydrodynamics". *Phys. Rev. Lett.,* **67**, pp. 3776–3779.

[14] Chen, S., and Doolen, G., 1998. "Lattice Boltzmann method for fluid flows". *Annu. Rev. Fluid Mech.,* **30**, pp. 329–364.

[15] He, X., and Luo, L.-S., 1997. "A priori derivation of the lattice Boltzmann equation". *Phys. Rev. E,* **55**, pp. 6333–6336.

[16] He, X., and Luo, L.-S., 1997. "Theory of the lattice Boltzmann method: From the Boltzmann equation to the lattice Boltzmann equation". *Phys. Rev. E,* **56**, pp. 6811–6817.

[17] Qian, Y., d'Humiéres, D., and Lallemand, P., 1992. "Lattice BGK models for the Navier-Stokes equations". *Europhys. Lett.,* **17**, pp. 479–484.

[18] Bhatnagar, P., Gross, E., and Krook, M., 1954. "A model for collision processes in gases. I. Small amplitude pro-

cesses in charged and neutral one-component system". *Phys. Rev.,* **94**, pp. 511–525.
[19] Alexander, F. J., Chen, S., and Sterling, J., 1992. "Lattice Boltzmann thermohydrodynamics". *Phys. Rev. E,* **47**, pp. 2249–2252.
[20] Chen, H., Molving, K., and Teixeira, C., 1997. "Digital Physics approach to computational fluid dynamics: some basic theoretical features". *Int. J. Mod. Phys. C,* **8**, pp. 675–684.
[21] Shan, X., and He, X., 1998. "Discretization of the velocity space in the solution of the Boltzmann equation". *Phys. Rev. Lett.,* **80**(1), pp. 65–68.
[22] Chen, H., and Teixeira, C., 2000. "H-thorem and origins of instability in thermal lattice Boltzmann models". *Computer Physics Communications,* **129**, pp. 21–31.
[23] Hänel, D., 2004. *Molekulare Gasdynamik*. Springer Verlag.
[24] Chapman, S., and Cowling, T., 1990. *The Mathematical Theory of Non-Uniform Gases*. Cambridge University Press.
[25] Succi, S., 2001. *The Lattice Boltzmann Equation*. Oxford Science Publications, New York.
[26] Zhou, Y., Zhang, R., Staroselsky, I., and Chen, H., 2004. "Numerical simulation of laminar and turbulent buoyancy-driven flows using a lattice boltzmann based algorithm". *Int. J. of Heat and Mass Transfer,* **47**, pp. 4869–4879.
[27] Schlichting, H., and Gersten, K., 1997. *Grenzschicht-Theorie*, 9 ed. Springer-Verlag, Berlin/Heidelberg/New York.
[28] Baehr, H. D., and Stephan, K., 1994. *Wärme- und Stoffübretragung*. Springer-Verlag, Berlin/Heidelberg.
[29] VDI, 1997. *VDI-Wärmeatlas*, 8 ed. Springer-Verlag, Berlin/Heidelberg.
[30] Wilcox, D. C., 1998. *Turbulence Modeling for CFD*, second ed. DCW Industries.
[31] Yakhot, V., Orszag, S. A., and Yakhot, A., 1987. "Heat transfer in turbulent fluids. i - pipe flow". *International Journal of Heat and Mass Transfer,* **30**, pp. 15–22.
[32] Pervaiz, M. M., and Teixeira, C. M., 1999. "Two equation turbulence modeling with the lattice-Boltzmann method". In Proc. o. ASME PVP Division Conference, Boston.
[33] Zhang, R., and Chen, H., 2003. "Lattice boltzmann method for simulations of liquid-vapor thermal flows". *Phys. Rev. E,* **67**, p. 066711.
[34] Succi, S., Amati, G., and Benzi, R., 1995. "Challenges in lattice Boltzmann computing". *J. Stat. Phys.,* **81**(1/2), pp. 5–16.
[35] Yakhot, V., Orszag, S. A., Thangam, S., Gatski, T. B., and Speziale, C. G., 1992. "Development of turbulence models for shear flows by a double expansion technique". *Phys. Fluids A,* **4**(7), pp. 1510–1520.
[36] Teixeira, C. M., 1998. "Incorporating turbulence models into the lattice-Boltzmann method". *Int. J. Modern Physics C,* **9**(8), pp. 1159–1175.
[37] Menter, F. R., Kuntz, M., and Bender, R., 2003. "A scale-adaptive simulation model for turbulent flow predictions". AIAA Paper 2003-0767.
[38] Chen, H., Kandasamy, S., Orszag, S., Shock, R., Succi, S., and Yakhot, V., 2003. "Extended Boltzmann kinetic equation for turbulent flows". *Science,* **301**, pp. 633–636.
[39] Fillipova, O., and Hänel, D., 1998. "Grid refinement for Lattice-BGK models". *J. Computat. Phys.,* **147**, pp. 219–228.
[40] Chen, H., Teixeira, C., and Molving, K., 1998. "Realization of fluid boundary condition via discrete Boltzmann dynamics". *Int. J. Mod. Phys. C,* **9**, pp. 1281–1292.
[41] White, F. M., 1991. *Viscous Fluid Flow*, second ed. McGraw-Hill.
[42] Alexander, C. G., H. Chen, S. K., Shock, R. A., and Govindappa, S. R., 2001. "Simulations of engineering thermal turbulent flows using a lattice Boltzmann based algorithm". In ASME PVP, Proc. of the 3rd Int. Symp. on Computational Technologies for Fluid/Thermal/Chemical/Stress Systems with Industrial Applications.
[43] Yu, D., Mei, R., and Shyy, W., 2002. "A multi-block lattice Boltzmann method for viscous fluid flow". *Int. J. Numer. Meth. Fluids,* **39**, pp. 99–120.
[44] Chen, H., 1998. "Volumetric formulation of the lattice Boltzmann method for fluid dynamics: Basic concept". *Phys. Rev. E,* **58**, pp. 3955–3963.
[45] Chen, H., Filippova, O., Hoch, J., Molving, K., Shock, R., Teixeira, C., and Zhang, R., 2006. "Grid refinement in lattice Boltzmann methods based on volumetric formulation". *Physica A,* **362**, pp. 158–167.
[46] Freed, D., 1998. "Lattice boltzmann method for macroscopic porous media modeling". *Int. H. Mod. Physics C,* **9**.
[47] Potthoff, J., and Wiedemann, J., 2003. "Die strassnfahrt-simulation in den ivk-windkanälen - ausführung und erste ergebnisse". 5th Stuttgart International Symposium, Expert-Verlag, Renningen. ISBN 3-8169-2180-9.
[48] Committee, S. R. V. A., 1994. "Aerodynamic testing of road vehicles - open throat wind tunnel adjustment". SAE Report J2071, Detroit.
[49] Kuthada, T., Genger, M., Widdecke, N., and Wiedemann, J., 2005. "Untersuchungen zu einem optimierten khlsystem". 6th Stuttgart International Symposium, Expert-Verlag, Renningen. ISBN 3-8169-2486-7.
[50] Schröeck, D., 2005. "Implementierung eines Programms zur Durchführung und Auswertung von Strömungsfeldmessungen im IVK-Modellwindkanal". Diploma Thesis, Institut für Verbrennungsmotoren und Kraftfahrwesen, Universität Stuttgart.